

### EUROFUSION WPMST1-PR(16) 15375

M Dunne et al.

# The role of the density profile in the ASDEX-Upgrade pedestal structure

Preprint of Paper to be submitted for publication in 43rd European Physical Society Conference on Plasma Physics (EPS)



This work has been carried out within the framework of the EUROfusion Consortium and has received funding from the Euratom research and training programme 2014-2018 under grant agreement No 633053. The views and opinions expressed herein do not necessarily reflect those of the European Commission.

This document is intended for publication in the open literature. It is made available on the clear understanding that it may not be further circulated and extracts or references may not be published prior to publication of the original when applicable, or without the consent of the Publications Officer, EUROfusion Programme Management Unit, Culham Science Centre, Abingdon, Oxon, OX14 3DB, UK or e-mail Publications.Officer@euro-fusion.org

Enquiries about Copyright and reproduction should be addressed to the Publications Officer, EUROfusion Programme Management Unit, Culham Science Centre, Abingdon, Oxon, OX14 3DB, UK or e-mail Publications.Officer@euro-fusion.org

The contents of this preprint and all other EUROfusion Preprints, Reports and Conference Papers are available to view online free at http://www.euro-fusionscipub.org. This site has full search facilities and e-mail alert options. In the JET specific papers the diagrams contained within the PDFs on this site are hyperlinked

## The role of the density profile in the ASDEX-Upgrade pedestal structure

- M. G. Dunne<sup>1</sup>, S. Potzel<sup>1</sup>, F. Reimold<sup>2</sup>, M. Wischmeier<sup>1</sup>, E. Wolfrum<sup>1</sup>, L. Frassinetti<sup>3</sup>, M. Beurskens<sup>4</sup>, P. Bilkova<sup>5</sup> M. Cavedon<sup>1,6</sup>, R. Fischer<sup>1</sup>,
- B. Kurzan<sup>1</sup>, F. M. Laggner<sup>7</sup>, R. M. McDermott<sup>1</sup>, G. Tardini<sup>1</sup>, E. Trier<sup>1</sup>,
- E. Viezzer<sup>1</sup>, M. Willensdorfer<sup>1</sup>, the EUROfusion MST1 Team<sup>8</sup>, and the ASDEX-Upgrade Team<sup>1</sup>

E-mail: mike.dunne@ipp.mpg.de

Abstract. Experimental evidence for the impact of a region of high density localised in the high-field side scrape-off layer (the HFSHD) on plasma confinement is shown in various dedicated experiments on ASDEX Upgrade (AUG). Increasing main ion fuelling is shown to increase the separatrix density and shift the density profile outwards. Predictive pedestal modelling of this shift indicates a 25 % decrease in the attainable pedestal top pressure, which compares well with experimental observations in the gas scan.

Since the HFSHD can be mitigated by applying nitrogen seeding, a combined scan in fuelling rate, heating power, and nitrogen seeding is presented. Significant increases in the achievable pedestal top pressure are observed with seeding, in particular at high heating powers, and are correlated with inward shifted density profiles and a reduction of the HFSHD and separatrix density. Interpretive linear stability analysis also confirms the impact of a radially shifted pressure profile on peeling-ballooning stability, with an inward shift allowing access to higher pressure gradients and pedestal widths.

<sup>&</sup>lt;sup>1</sup>Max-Planck-Institut für Plasmaphysik, D-85748 Garching, Germany

<sup>&</sup>lt;sup>2</sup>Forschungszentrum Jülich, D-52425 Jülich, Germany

<sup>&</sup>lt;sup>3</sup>Division of Fusion Plasma Physics, Association EURATOM-VR, KTH, SE-10044 Stockholm, Sweden

<sup>&</sup>lt;sup>4</sup>Max-Planck-Institut für Plasmaphysik, D-85748 Greifswald, Germany

<sup>&</sup>lt;sup>5</sup>Institute of Plasma Physics, Prague, Hlavni Mesto, Praha, Czech Republic

<sup>&</sup>lt;sup>6</sup>Physik-Department E28, Technische Universität München, Garching Germany

<sup>&</sup>lt;sup>7</sup>Institute of Applied Physics, TU Wien, Fusion@ÖAW, 1040 Vienna, Austria

<sup>&</sup>lt;sup>8</sup> See http://www.euro-fusionscipub.org/mst1

#### 1. Introduction

The impact of divertor conditions on pedestal structure and, hence, global confinement has become clear in recent years through extensive experiments with main ion fuelling and impurity seeding on ASDEX Upgrade (AUG)[1, 2] and JET[3, 4]. Many experiments have been conducted varying only the main ion gas fuelling over a power scan and have reported a significant degradation of global confinement, which has been linked to a reduction of the pedestal top pressure ( $p_{ped}$ ) values[4, 5, 6]. At the same time, nitrogen seeding has generally been shown to improve  $p_{ped}$  in metal-walled machines[3, 7].

Several experimental and theoretical studies have attempted to determine the mechanism(s) for this confinement loss. So far, attempts have focussed either on the change of  $Z_{\rm eff}$  as a driving mechanism[8], or the change of separatrix temperature[9]. However, one parameter which links the effect of fuelling and seeding on scrape-off layer (SOL) parameters is the high-field-side high-density front (HFSHD)[10], a poloidally localised region of high density located in the HFS SOL and extending from the x-point towards the midplane. This front appears when gas fuelling is applied at sufficient heating power and the density in it reduces with impurity seeding; this is due to the radiation of the exhausted power before it reaches the HFS SOL and ionises the particles associated with the HFSHD. A reduction of heating power also has a similar effect.

Since the density in this front is approximately one order of magnitude higher than the separatrix density, and also due to its proximity to the separatrix between the x-point and inner midplane, it can be expected to alter the fuelling of the plasma via diffusion or drift-based transport rather than any kind of neutral penetration effects[15]. If this is the case, the separatrix density would increase and the density profile could shift outwards, depending on the type of particle transport in the pedestal. Generally, density profiles are self similar, that is, they exhibit a critical gradient length (i.e. constant  $\nabla n \setminus n$ )[11, 12], implying that a higher density at the separatrix would lead to an effective outward shift of the density profile when the HFSHD is present.

Experiments to test this effect have been carried out on ASDEX Upgrade and the interpretation is presented here. Section 2 describes the HFSHD in more detail and also presents the impact it is expected to have on a peeling-ballooning limited Type-I ELMing pedestal. Section 3 shows analysis of selected experiments, and section 4 combines a wider database of discharges.

#### 2. Impact of HFSHD on density profile location and pedestal stability

In order to fully test the hypothesis that the density profile location, or, more accurately, the location of the steepest density gradient, is the dominant parameter for the pedestal, the actuators for its location must first be determined. It is hypothesised that the HFSHD dominates the location via an alteration of the fuelling pattern; therefore, we discuss in this section the experimental and modelling observations of the HFSHD, its dependencies, and the predicted impact on p<sub>ped</sub>.

Experimental evidence for the HFSHD was first obtained in the AUG tokamak[13]. Since then it has been investigated intensively in relation to the onset of detachment in AUG L-mode plasmas[10] and during H-mode operation in both AUG and JET[14]. The HFSHD is observed in discharges with a main ion gas puff and sufficient heating power. Scalings of the HFSHD show that its density increases with heating power crossing the separatrix, which is also supported by

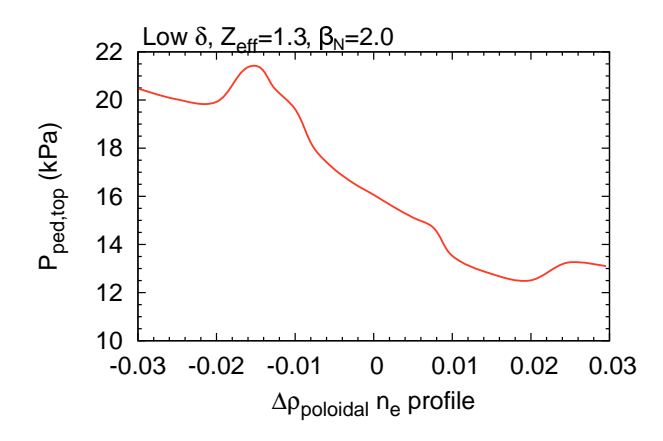


Figure 1: Predicted pedestal top pressure as a function of the position of the density profile location at constant global  $\beta$ , effective charge  $Z_{\rm eff}$ , and pedestal top density. The predicted  $p_{\rm ped}$  varies by  $\pm 25\%$  around the "0" shift value, with a shift of only  $0.01\rho_{\rm poloidal}$  being sufficient to produce such a result; this corresponds to a real-space shift of  $\sim 5$  mm in AUG.

the latest results from SOLPS modelling[15]. These results describe several key points about the nature of the HFSHD: first, it consists of plasma localised to the HFS SOL due to strong local recycling and drift-driven transport; secondly, these particles are ionised by a heat flux which is ejected from the LFS midplane (ad-hoc ballooning transport was assumed in models); and thirdly, if this heat flux is mitigated via, for example, nitrogen seeding, which increases the radiated power in the SOL, the HFSHD decreases. The modelling has also shown that the HFSHD increases with an increasing neutral gas puff.

Due to the high density in the HFSHD, up to one order of magnitude higher than the separatrix density, the nature of plasma fuelling changes. The HFSHD acts as a source for diffusive and drift-based fuelling of the plasma, increasing the density at the separatrix mainly on the HFS, but also measurably at the low-field side (LFS) midplane. The end result of increasing density at the separatrix is that the density profile experiences an effective outward shift, which can then be mitigated by nitrogen seeding.

Using the iPED predictive pedestal code[8], which mainly uses the same assumptions as the original EPED model[26] to derive the pedestal temperature and density shapes as well as the current density profile, the effect of shifting the mid-point of the density profile inwards and outwards was tested. A low triangularity plasma shape ( $\delta_{\rm av}=0.25$ ) was taken, which corresponds to the discharges performed in this paper. At a constant global  $\beta$ , effective charge  $Z_{\rm eff}$  and pedestal top density, the location of the density profile was scanned radially. Current density profiles consistent with this shifted location were then calculated for the range of pedestal top temperatures and all cases were tested for linear MHD stability, resulting in a maximum stable pedestal top pressure. The results of this scan are shown in figure 1.

From this figure we can expect an easily observable change of the achievable pedestal top pressure depending on the location of the density profile. The model predicts a  $\pm 25\%$  change of p<sub>ped</sub> when the density profile is shifted by just  $\Delta \rho_{\text{poloidal}} = 0.01$ , corresponding to 5 mm in real space in AUG. These results echo modelling predictions via profile shifts on JET[16, 9], NSTX[17], and DIII-D[18]. This will be tested both experimentally and via interpretive stability analysis in

the following section, which deals with the specific experiments to vary the HFSHD via gas puff, nitrogen seeding, and heating power.

#### 3. Variation of pedestal top with fuelling and seeding

#### 3.1. Fuelling scan

The degradation of global and pedestal confinement with a gas puff in H-modes has been well documented in both carbon[19] and, more extensively, in metal-walled devices[5, 4, 20]. In this section, we describe such an experiment on AUG, taking an H-mode plasma at 1 MA plasma current, -2.5 T toroidal field, 12 MW of heating power and a medium triangularity shape and varying the gas puff from 0.5 to 1.0 and  $2.0 \times 10^{22}$  e<sup>-s<sup>-1</sup></sup> (denoted hereafter as very low, low, and medium fuelling rates). Time traces of this discharge showing (a) the heating power and radiated power, (b) the deuterium fuelling rate, (c) the plasma density, (d) the plasma stored energy expressed as  $\beta_N$ , (e) the ELM frequency, and (f) the HFSHD are shown in figure 2. The grey points, which are data from a single line of sight from a Stark-broadening diagnostic[10] intersecting the HFSHD volume, are inter-ELM measurements of the electron density and the green line is a smooth running average of the time trace. Some ELM-related scatter is still visible in the data as the integration time of the diagnostic is 2.5 ms and part of the recovery from the ELM is captured.

The plasma stored energy decreases significantly between steps one and two and then only slightly between steps two and three. This is correlated with the change in the density contained in the HFSHD, which increases by 20 % between steps one and two and by only a few percent during the last step. To test the hypothesis of the density profile location, the experimental data from the AUG edge diagnostic suite[21] were analysed. Shown in figure 3 are the electron temperature (a) and density (b) profiles for the very low (black) and medium (red) fuelled phases. Since Thomson scattering data were used to fit both temperature and density in addition to ECE and lithium beam data, the profiles within one time step are automatically aligned to each other. Both temperature and density profiles are then shifted together such that the electron temperature at the separatrix is 100 eV, which is typical for AUG[22]. The temperature pedestal top has clearly reduced in height, which can be expected in a higher density plasma, but, critically, the density has not increased by enough to compensate this drop and conserve the pedestal top pressure. Instead, the density profile has shifted outwards in the medium fuelled case by approximately  $\Delta \rho_{\text{poloidal}} = 0.01$ , causing  $\rho_{\text{ped}}$  to reduce by 25 %, in good agreement with the model prediction from section 2.

To further verify this effect, linear stability analysis was conducted on the pedestals from all three time points. A scan in current density and pressure gradient was performed to determine the stability boundaries, following the methodology described in [8]. The resulting boundaries along with the operational points (maximum normalised pressure gradient  $\alpha$  and edge  $j_{\phi}$ ) are shown in figure 4. The figure clearly indicates that the expected operational space has shrunk for the time points at higher fuelling, in agreement with the movement of the operational points. There is some uncertainty in the determined stability boundaries, of the order of 10 %, but this is fairly typical of such analysis. The curtailing of the maximum allowed  $\alpha$  then results in a much reduced pedestal top value, as already illustrated in section 2.

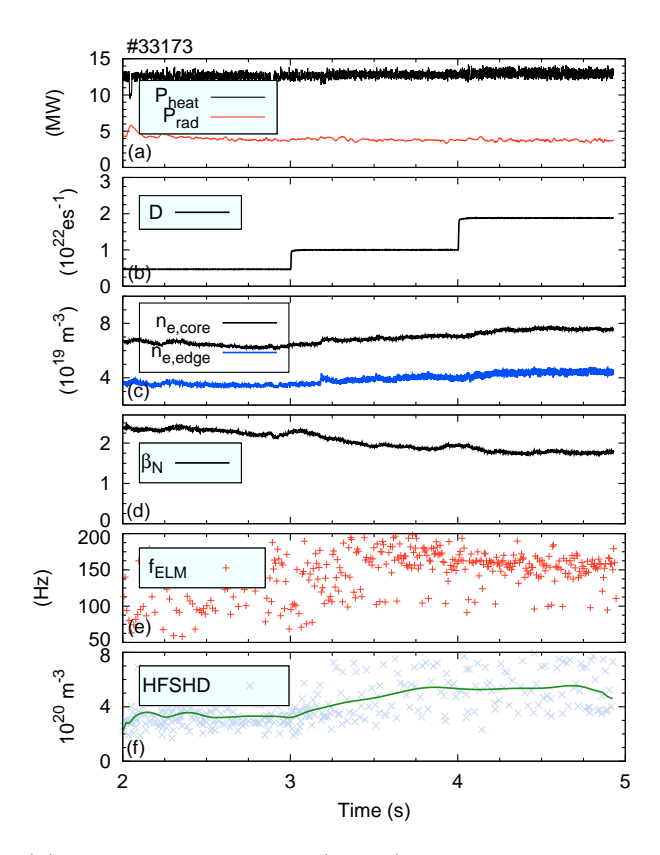
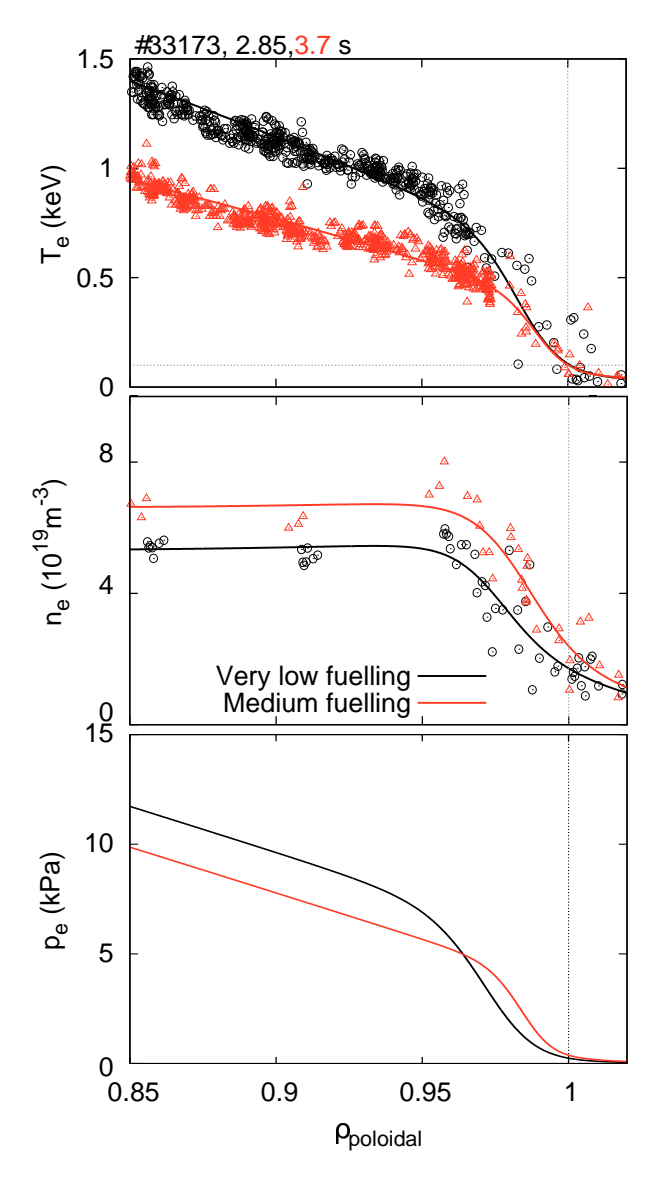


Figure 2: Time traces of (a) the heating power (black) and radiated power (red), (b) the deuterium fuelling rate, (c) the core (black) and edge (blue) plasma density, (d) the plasma stored energy expressed as  $\beta_N$ , (e) the ELM frequency, and (f) the HFSHD. As the fuelling rate is increased stepwise, the stored energy decreases. This is also correlated with the HFSHD, which increases by 20 % between steps one and two, and remains almost constant between steps two and three.

#### 3.2. Nitrogen seeding

Although increasing the fuelling rate and the HFSHD lead to a degradation of  $p_{ped}$ , the effect can be reversed. Confinement improvement via nitrogen seeding at JET-ILW[4, 3], Alcator C-Mod[5, 23], and AUG[8, 3, 1] have been well reported and documented, but so far without an explanation. Since many of these experiments have taken place in metal-walled devices with a gas puff to mitigate the effects of high-Z materials on plasma stability, it is likely that the reference scenarios shown in these papers have the HFSHD. Indeed, the plasma scenario used in this work is based on the one presented in the AUG references. Since we know that nitrogen seeding mitigates the HFSHD, it is possible that this is the parameter which dominates confinement improvement. While the record level of confinement improvement observed at AUG is 40% [2], levels of 25–30 % are quite typical[8].

An example of confinement improvement with nitrogen seeding is shown in figure 5. Heating power (a) is kept constant, as is the deuterium fuelling (b, black) while nitrogen seeding (green) is introduced after a reference peroid at 3 s. The plasma density (c) reacts only slightly, while a large change (+25%) in the global beta (d) is observed. The ELM frequency (e) is not significantly changed, though the scatter is increased and the ELM length is shortened, and the HFSHD (f) also decreases after nitrogen is introduced. This drop in the HFSHD and increase in stored energy



**Figure 3:** Profiles of (a) electron temperature and (b) electron density for the very-low (black) and medium (red) fuelled cases. The temperature pedestal decreases significantly with increased fuelling, and, while the density pedestal increase slightly compensates this, its outward shift results in a lower pedestal top pressure.

is exactly the opposite of what happened in the gas puff scan shown in the previous section; we will now analyse the experimental profiles and pedestal stability to determine if the confinement change mechanism is the same.

Shown in figure 6 are (a) temperature and (b) density profiles for discharge #31228 for reference (red) and nitrogen seeded (blue) time points. As in section 3.1, the temperature profiles have been aligned such that  $T_{\rm e,sep}$ =100 eV and the density profiles are then automatically aligned to these temperature profiles via Thomson Scattering. In this case, when nitrogen seeding is applied the HFSHD shrinks in magnitude and the density profile shifts radially inwards again. Interpretive stability analysis in this case shows that both time points are consistent with the peeling-ballooning model, but indicates no change in the critical  $\alpha$  value; as pointed out in [18],

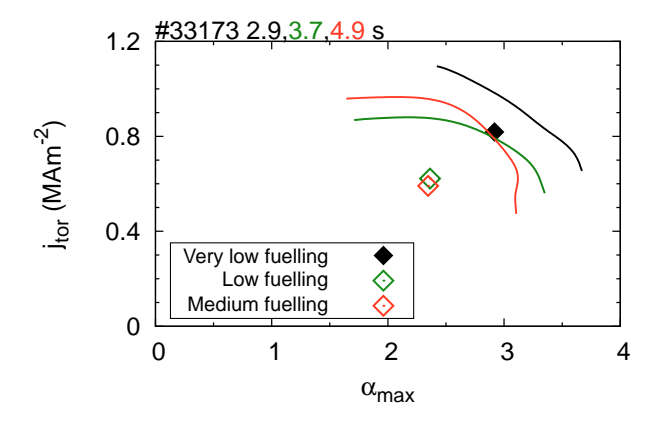
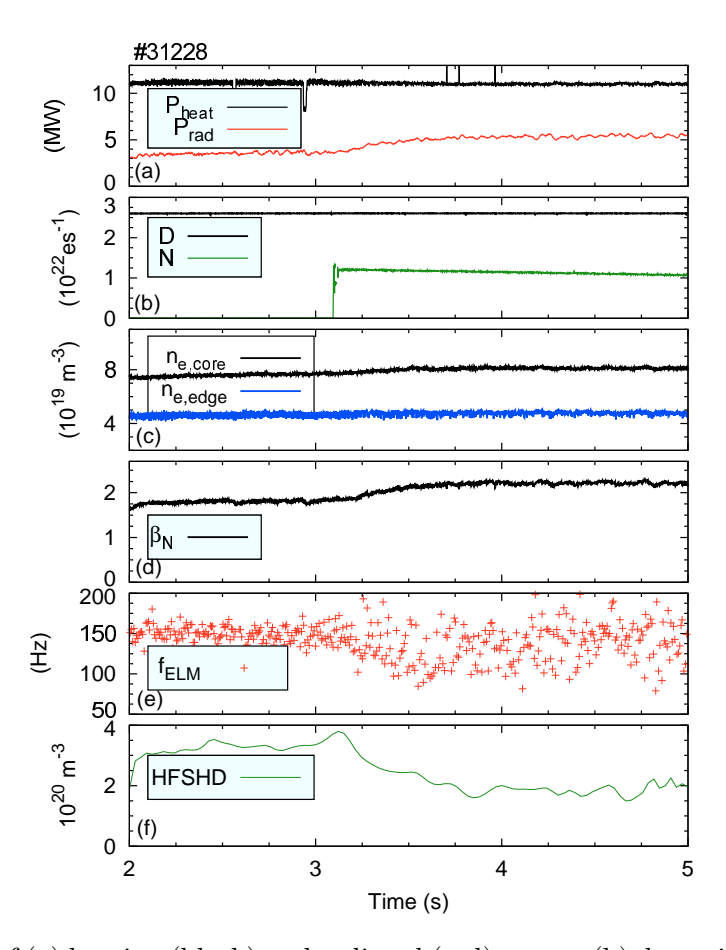
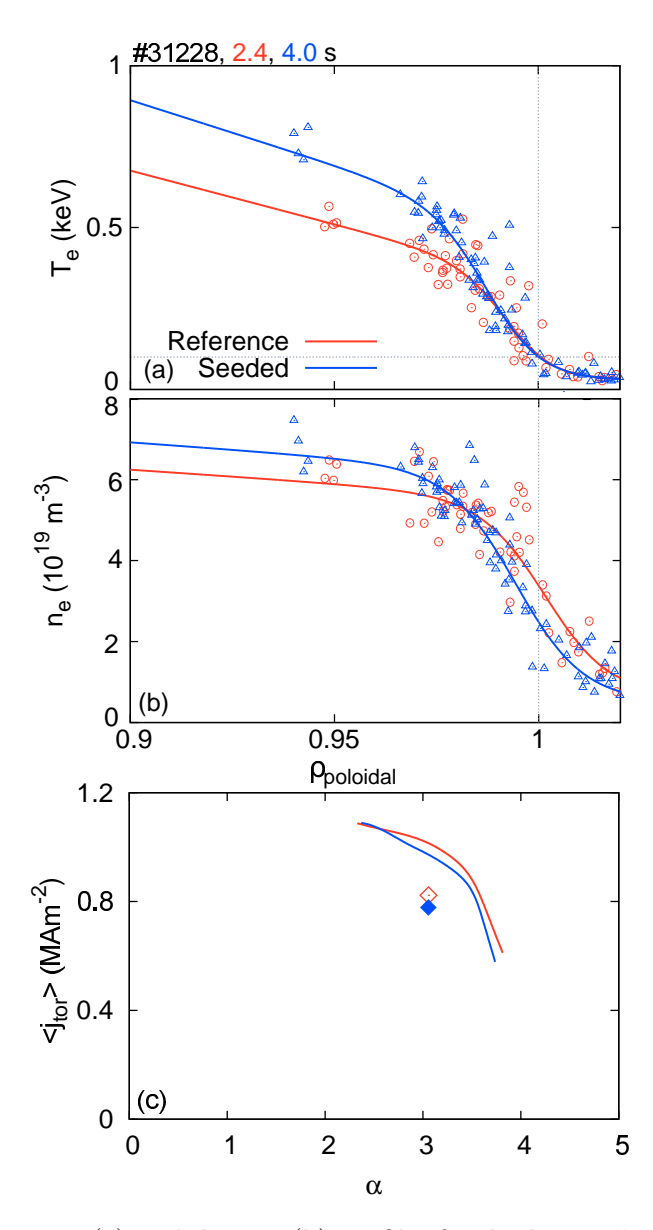


Figure 4: j- $\alpha$  stability boundaries for the three phases of discharge #33173 (lines) with the operational points (diamonds). Access to higher pressure gradients and current densities is restricted in the higher fuelled cases, resulting in a lower pedestal top pressure.



**Figure 5:** Time traces of (a) heating (black) and radiated (red) power, (b) deuterium (black) and nitrogen (green) gas puff rates, (c) core (black) and edge (blue) line integrated densities, (d) global normalised  $\beta$ , (e) ELM frequency, and (f) the density in the HFSHD. As nitrogen seeding is added and radiated power is increased, the density in the HFSHD decreases and confinement improves.



**Figure 6:** Electron temperature (a) and density (b) profiles for discharge #31228 for reference (red) and nitrogen seeded (blue) time points. When nitrogen is seeded the density profile shifts radially inwards, allowing a higher pedestal top pressure. Stability diagrams (c) for both time points show consistency with the peeling-ballooning model, but no significant difference in the stability boundaries can be discerned.

since  $\alpha$  contains a factor of  $q^2$  (where q is the safety factor), this will still result in a higher real space pressure gradient since the peak gradient is now centered around a lower q value.

To observe the impact of a radial shift over a wider range of conditions, the high gas points (D fuelling level of  $2.7 \times 10^{22} \mathrm{e^-s^{-1}}$ ) with a variation in the seeding rate and heating power were chosen. A detailed overview of the database is presented in [8]. Figure 7 shows the impact of increasing  $Z_{\mathrm{eff}}$  via nitrogen seeding on the location of the density profile; the HFSHD is reduced with increasing nitrogen seeding and the density profile shifts radially inwards with a reduction in the separatrix density. It is important to distinguish the causality in this case. When nitrogen is seeded,  $Z_{\mathrm{eff}}$  in the main plasma increases and the radiated power in the SOL also increases. It

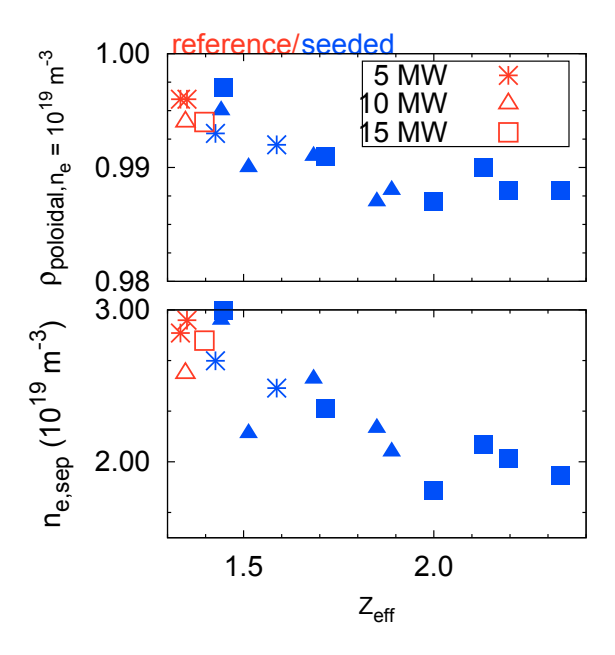


Figure 7: (a) Inward movement of the density profile depending on  $Z_{eff}$  and (b) decrease of the separatrix density with increasing  $Z_{eff}$ . All data points are at the high gas fuelling rate.

is the radiated power increase which acts to decrease the HFSHD[14, 15]; an increased  $Z_{eff}$  is a side-effect of the methodology used. The position of the density profile is taken as the location of a specific density layer  $(3.5 \times 10^{19} \text{m}^{-3})$ , which accurately describes the profile location at high gas since the pedestal top density and peak gradient do not change significantly; this is not the case for the lower gas scans. For the fuelling rate shown here, the maximum movement of the density profile is  $\Delta \rho_{\text{poloidal}} = 0.01$ , while over the entire dataset of gas, power, and nitrogen seeding scans, it is approximately  $\Delta \rho_{\text{poloidal}} = 0.015$ . This reduction of the separatrix density then allows a higher  $p_{\text{ped}}$  to be obtained for otherwise similar paramters (pedestal top density and constant input power; three powers are shown in figure 7). From this point onwards, only the separatrix density will be used to show the impact of the HFSHD on  $p_{\text{ped}}$ .

#### 4. Combined gas, power, and seeding scan

One of the often quoted findings of the ITER-98 confinement time scaling is a so-called power degradation, in that the expected confinement time decreases as  $P_{\text{net}}^{-0.69}$ . This is not so desireable as it implies that the expected confinement gets worse at higher input powers. However, many scans indicate that this may be a somewhat pessimistic view[11, 24, 6] and show a much weaker power degradation in individual scans of just the power. In particular, Maggi et al.[6] show a significant difference in the power degradation at different fuelling levels, with low fuelling plasmas having a much lower degradation than highly fuelled plasmas; the difference in confinement in those cases also stemmed from a change in the pedestal top pressure. They also show that the difference in achievable  $p_{\text{ped}}$  increases at higher heating power, correlating well with the idea that the HFSHD is acting to reduce the achievable pedestal top pressure.

The pedestal top pressure  $p_{ped}$  as a function of fuelling level and impurity seeding is also investigated here for three fuelling rates  $(1.0,2.0,2.7\times10^{22}e^-s^{-1})$ , low, medium, high fuelling) in

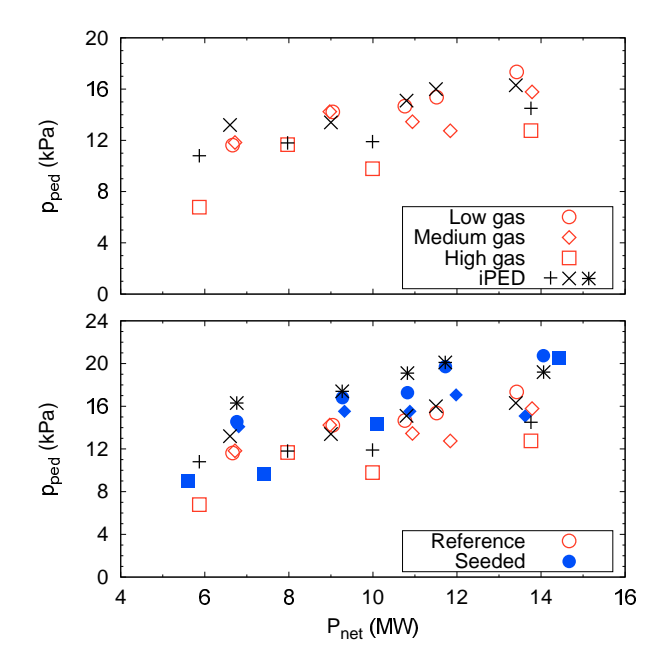
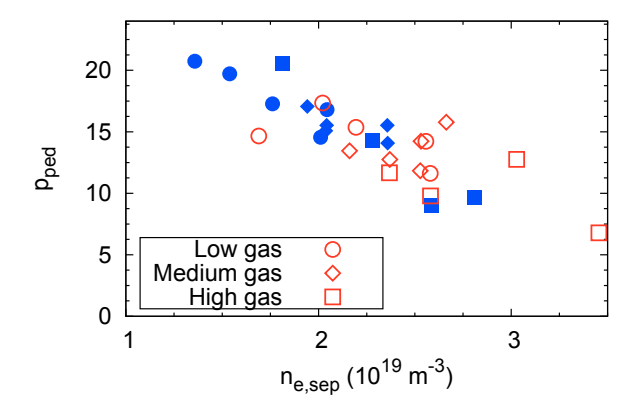


Figure 8: Pedestal top pressure as a function of input power for (a) reference only datapoints in the gas scan and (b) additional nitrogen seeded points overlayed in blue. Results of iPED analysis of the low gas reference points (red circles) are also shown as  $\times$ , while the high gas iPED results (including an radial outward shift 0f  $\Delta \rho_{\text{poloidal}} = 0.01$ ) are shown as +. The outward shift is required to reproduce the lower pedestal top values in the high gas cases. iPED analysis of the low gas, nitrogen seeded points are also shown as \*; these points were run with  $Z_{\text{eff}} = 2.0$  and a slight inward shift ( $\Delta \rho_{\text{poloidal}} = 0.005$ .)

a power scan ranging between 6-15 MW. Various levels of nitrogen seeding were applied and the highest  $p_{ped}$  with a global  $\beta_N$  below 2.7 for each power/gas combination will be shown in the following figures. Figure 8 shows the measured pedestal top pressure as a function of input heating power for three gas levels (low, medium, and high, shown as circles, diamonds, and squares, respectively). While  $p_{ped}$  increases with heating power, it varies significantly with fuelling. In particular, there are large differences between the low and high gas data points. Also shown as black crosses are the iPED predictions for the low gas puff; the model in this case predicts the general trend of the pedestal with global beta and pedestal density. The iPED predictions for the high gas scans are also shown as the black "+" symbols; an outward density profile shift of  $\Delta \rho_{poloidal} = 0.01$  was included for these points. The slight changes in plasma beta and pedestal top density were not enough to recover the significantly lower pedestal top values while including the radial shift of the density profile gives almost the correct value of  $p_{ped}$ .

The impact of nitrogen seeding on  $p_{ped}$  is shown in figure 8(b) as the blue symbols overlayed on the reference data with the same shape coding as for the gas puff scan. The predicted pedestal top pressure values for the low gas seeded points are shown as the "\*" symbols. In this case, a small inward shift of  $\Delta\rho_{poloidal}=0.005$  was used across the entire power range, as well as an increased  $Z_{eff}$  of 2.0. Good agreement is observed between the increased pedestal top in the experiment and in the modelling across the three subsets. A discrepancy does exist between the model and experiment in the low-power, high gas puff points, with the model overestimating, the pedestal top value; other effects such as the exact shape of the density profile are being investigated to resolve this issue. In general, the strongest dependence of the pedestal top is on where the location of the



**Figure 9:** Dependence of the pedestal top pressure on the separatrix density for the full database of discharges. Regardless of the method of separatrix density change (gas puffing or nitrogen seeding) the data are well ordered by this parameter alone.

density profile. This is further indicated in figure 9, which plots the pedestal top pressure for the entire gas, power, and nitrogen seeding scan as a function of the separatrix density.

This decrease of  $p_{ped}$  with increasing separatrix density echos one already found on Alcator C-Mod[11, 5], that the pedestal top pressure and global confinement depend strongly on the separatrix density and, in particular, on the location of the density profile relative to the separatrix. Since the C-Mod studies were undertaken in EDA H-mode, and the ones presented here were made in Type-I ELMing H-modes, it seems to be a general feature of the edge pedestal; this is perhaps not surprising since both EDA H-mode and the ELMing pedestal are thought to be predominantly ballooning limited[25, 26] (or, at least, consistent with ballooning scalings) and the shift of the pressure profile relative to the separatrix has a strong impact on ballooning stability. This result indicates that the profile shift should be considered in all modes of operation featuring an edge pedestal, including Type-II and other small-ELM regimes which generally scale in a ballooning-like fashion.

#### 5. Conclusions

In this paper we have presented the experimental findings on the impact of the high-field-side high-density on ASDEX Upgrade on the density profile, its location relative to the separatrix, and the subsequent impact on pedestal stability. Increasing the density in the HFSHD, mainly by main ion fuelling, causes an increase of diffusive and drift driven fuelling of the plasma, causing a higher separatrix density and consequently effectively shifting the pedestal density radially outwards. Conversely, reducing this density by nitrogen seeding reduces the separatrix density and allows the density profile to shift back inwards. Predictive pedestal modelling shows that a radial shift of  $\Delta \rho_{poloidal} = 0.01$ , or 5 mm in AUG, is sufficient to alter the pedestal top pressure by  $\pm 25\%$ . Measurements of the temperature and density profiles in a gas fuelling scan are consistent with this picture, with the density profile shifting outwards and the pedestal, and, hence, global confinement reducing.

Introducing nitrogen seeding into these degraded plasmas has been shown to shift the density

profile inwards and is well correlated with the pedestal top pressure in a wide range of heating powers, fuelling rates, and nitrogen seeding rates. Although the EPED model captures much of the basic physical properties of the pedestal, this work has shown that it is quite important to also consider such fuelling effects in order to accurately predict the pedestal. If this effect can be used to reduce the uncertainties in such predictive models is, as yet, unclear. A theoretical framework to predict, at least to leading order, how the density profile forms is required for such a predictive model.

#### Acknowledgement

This work has been carried out within the framework of the EUROfusion Consortium and has received funding from the Euratom research and training programme 2014-2018 under grant agreement No 633053. The views and opinions expressed herein do not necessarily reflect those of the European Commission.

#### References

- [1] J. Schweinzer, A.C.C. Sips, G. Tardini, et al. Nuclear Fusion, 51(11):113003, nov 2011.
- [2] A. Kallenbach, M. Bernert, R. Dux, et al. Plasma Physics and Controlled Fusion, 55(12):124041, dec 2013.
- [3] M.N.A. Beurskens, J. Schweinzer, C. Angioni, et al. *Plasma Physics and Controlled Fusion*, 55(12):124043, dec 2013.
- [4] C Giroud, S Jachmich, P Jacquet, et al. Plasma Physics and Controlled Fusion, 57(3):035004, mar 2015.
- [5] J.W. Hughes, a. Loarte, M.L. Reinke, et al. Nuclear Fusion, 51(8):083007, aug 2011.
- [6] C.F. Maggi, S. Saarelma, F.J. Casson, et al. Nuclear Fusion, 55(11):113031, sep 2015.
- [7] M.L. Reinke, J.W. Hughes, a. Loarte, et al. Journal of Nuclear Materials, 415(1):S340–S344, aug 2011.
- [8] M.G. Dunne, L. Frassinetti, M.N.A. Beurskens, et al. Submitted to Plasma Physics and Controlled Fusion, 2016.
- [9] S. Saarelma, A. Järvinen, M. Beurskens, et al. Physics of Plasmas, 22(5):056115, may 2015.
- [10] S. Potzel, M. Wischmeier, M. Bernert, et al. Nuclear Fusion, 54(1):013001, jan 2014.
- [11] J.W Hughes, B LaBombard, J Terry, et al. Nuclear Fusion, 47(8):1057-1063, aug 2007.
- [12] P.A. Schneider, E. Wolfrum, R.J. Groebner, et al. Nuclear Fusion, 53(7):073039, jul 2013.
- [13] K. McCormick, R. Dux, R. Fischer, et al. Journal of Nuclear Materials, 390-391:465-469, jun 2009.
- [14] S. Potzel, M. Wischmeier, M. Bernert, et al. Journal of Nuclear Materials, pages 8–12, dec 2014.
- [15] F. Reimold, M. Wischmeier, S. Potzel, et al. Submitted to Nuclear Materials and Energy, 2016.
- [16] J.-S. Lönnroth, V. Parail, D.C. McDonald, et al. Nuclear Fusion, 51(1):013003, 2011.
- [17] R. Maingi, S. M. Kaye, C. H. Skinner, et al. Physical Review Letters, 107(14):145004, sep 2011.
- [18] T.H. Osborne, G.L. Jackson, Z. Yan, et al. Nuclear Fusion, 55(6):063018, jun 2015.
- [19] M.N.a. Beurskens, L. Frassinetti, C. Challis, et al. Nuclear Fusion, 53(1):013001, jan 2013.
- [20] C.F. Maggi, E. Delabie, T.M. Biewer, et al. Nuclear Fusion, 54(2):023007, feb 2014.
- [21] E. Wolfrum, E. Viezzer, a. Burckhart, et al. Nuclear Fusion, 55(5):053017, may 2015.
- [22] J. Neuhauser, D Coster, HU Fahrbach, et al. Plasma Physics and Controlled Fusion, 44(6):855-869, 2002.
- [23] A. Loarte, J. W. Hughes, M. L. Reinke, et al. Physics of Plasmas, 18(5):056105, 2011.
- [24] C.D. Challis, J. Garcia, M. Beurskens, et al. Nuclear Fusion, 55(5):053031, may 2015.
- [25] J. W. Hughes, D. a. Mossessian, a. E. Hubbard, et al. Physics of Plasmas, 9(7):3019, 2002.
- [26] P.B. Snyder, R.J. Groebner, J.W. Hughes, et al. Nuclear Fusion, 51(10):103016, oct 2011.